

Electronic Delivery Cover Sheet

NOTICE WARNING CONCERNING COPYRIGHT RESTRICTIONS

The copyright law of the United States (Title 17, United States Code) governs the making of photocopies or other reproductions of copyrighted materials.

Under certain conditions specified in the law, libraries and archives are authorized to furnish a photocopy or other reproduction. One of these specified conditions is that the photocopy or reproduction is not to be "used for any purpose other than private study, scholarship, or research." If a user makes a request for, or later uses, a photocopy or reproduction for purposes in excess of "fair use," that user may be liable for copyright infringement.

This institution reserves the right to refuse to accept a copying order if, in its judgment, fulfillment of the order would involve violation of copyright law.

This notice is posted in compliance with Title 37 C. F. R., Chapter II, Part 201.14



Rapid #: -22662070

CROSS REF ID: 1729796

LENDER: CSF (San Francisco State Univ.) :: Leonard Library

BORROWER: VPI (Virginia Tech) :: Newman Library

TYPE: Article CC:CCG

JOURNAL TITLE: Archives of biochemistry and biophysics

USER JOURNAL TITLE: Archives of Biochemistry and Biophysics

ARTICLE TITLE: Kinetic characterization of a flavin-dependent monooxygenase from the insect food crop pest,

Zonocerus variegatus

ARTICLE AUTHOR: Sydney B. Johnson a, Kathryn Paasch a, Starlina Sh

VOLUME: 754

ISSUE:

MONTH:

YEAR: 2024

PAGES: 109949

ISSN: 1096-0384

OCLC #:

Processed by RapidX: 6/3/2024 10:40:54 AM

This material may be protected by copyright law (Title 17 U.S. Code)



Contents lists available at ScienceDirect

Archives of Biochemistry and Biophysics

journal homepage: www.elsevier.com/locate/yabbi





Kinetic characterization of a flavin-dependent monooxygenase from the insect food crop pest, *Zonocerus variegatus*

Sydney B. Johnson a, Kathryn Paasch , Starlina Shepard a, Pablo Sobrado a,b,*

ABSTRACT

Zonocerus variegatus, or the painted grasshopper, is a food crop pest endemic in Western and Central Africa. Agricultural industries in these regions rely heavily on natural defense mechanisms to control the grasshopper population such as plant-secreted alkaloid compounds. In recent years, the *Z. variegatus* population has continued to rise due to acquired resistance to alkaloids. Here we focus on the kinetic characterization of a flavin-dependent monooxygenase, ZvFMO, that catalyzes the nitrogen oxidation of many of these alkaloid compounds and confers resistance to the insect. Expression and purification of ZvFMO through a traditional *E. coli* expression system was successful and provided a unique opportunity to characterize the catalytic properties of an FMO from insects. ZvFMO was found to catalyze oxidation reactions of tertiary nitrogen atoms and the sulfur of cysteamine. Using stopped-flow spectroscopy, we have determined the kinetic mechanism of ZvFMO. We assessed F383 for its involvement in substrate binding, which was previously proposed, and determined that this residue does not play a major role in binding substrates. Through molecular docking, we identified N304 and demonstrated that this residue plays a role in substrate binding. The role of K215 was studied and was shown that it plays a critical role in NAD(P)H binding and cofactor selectivity.

1. Introduction

In Western and Central Africa, the population of Zonocerus variegatus has continued to climb and was declared a major food crop pest by Nigeria in the 1970s, but crop damages have been reported as early as 1910 [1]. The consumption of crops and egg laying on crops by Z. variegatus has resulted in major losses of banana and cassavas crops, ranging widely from 10% to 80% losses in annual yields [1]. In addition, Z. variegatus has also been implicated as a vector for plant disease by its association with bacterial blight in cassavas and in the transmission of mosaic viruses to okra [1]. To date, farmers have been reported to use three major methods of population control: 1) natural defense; 2) chemical defense; and 3) physical control [1,2]. Chemical defense mechanisms include the use of expensive insecticides that are often harmful to the environment, while physical control often includes the removal of the eggs and the adult insects through various techniques [1, 2]. Natural defense mechanisms often rely on the secretion of alkaloid compounds. These compounds are secreted by the plant in their nontoxic N-oxidized form and are reduced to their protoxic free base form by the reducing environment of the insect gut [3] (Scheme 1).

Recently, flavin-dependent monooxygenases (FMOs) from the Lepidoptera and Orthoptera insect orders have been identified to carry out the detoxifying oxidation of pyrrolizidine alkaloids [3]. The free base form of alkaloids in the pyrrolizidine family have been shown to have potent genotoxic effects in insects, aiding in the plant-defense against herbivores such as *Z. variegatus* [4]. The resistance to these compounds conferred by the FMO makes the enzymes attractive drug targets for the specific defense against herbivorous insects. A lack of enzyme solubility has limited extensive characterization of these FMOs, but an FMO from *Z. variegatus*, ZvFMO (also referred to as ZvPNO in other works) has been identified as a suitable candidate for recombinant expression and purification from *E. coli* and downstream characterization [3,5,6].

The FMO family is vast and catalyzes diverse oxidation reactions of xenobiotic compounds and can play roles in biosynthesis pathways [7, 8]. Based on their structure and mechanism, FMOs are divided into eight subclasses (A-H) [8]. The crystal structure of ZvFMO was solved in 2018 with FAD and NADP⁺ bound [9]. The structure is consistent with ZvFMO being a member of class B. Class B FMOs feature two nucleotide binding Rossman-folds and are the only FMO class that retain the NADP⁺ after reduction [8,10]. Their reaction mechanism can be separated into two parts: the reductive-half and oxidative-half reactions. Key features of the class B reductive-half reaction are that the rate constant of reduction is not enhanced by substrate binding and that the flavin is directly reduced by NADPH without the need for an external reductase [8,11]. The class B oxidative-half reaction features a stable C4a-(hydro)peroxyflavin, which serves as the oxygenating species of soft nucleophiles such as nitrogen or

a Department of Biochemistry, Virginia Tech. Blacksburg, VA. 24061, USA

^b Center for Drug Discovery, Virginia Tech, Blacksburg, VA, 24061, USA

^{*} Corresponding author. Department of Biochemistry and Center for Drug Discovery, Virginia Tech, Blacksburg, VA, 24061, USA. *E-mail addresses*: sbj2001@vt.edu (S.B. Johnson), kathrynpaasch@vt.edu (K. Paasch), star@vt.edu (S. Shepard), psobrado@vt.edu (P. Sobrado).

sulfur atoms [12–14]. This species is stabilized by the bound NADP⁺, which is released at the end of the catalytic cycle along with the product [13].

In this work, we aimed to determine the kinetic mechanism of ZvFMO, which will serve as the first detailed kinetic characterization of an FMO from an insect. Anaerobic time-resolved spectroscopy experiments demonstrated high affinity for NADPH and a fast flavin reduction step along with a very stable C4a-(hydro)peroxyflavin in the absence of substrate. Our results demonstrated that flavin oxidation and/or product/NADP+ release are the rate-limiting steps. Previous work determined that ZvFMO has activity with a variety of tertiary nitrogencontaining substrates and with cysteamine [5]. In agreement with previous work, we found that ZvFMO catalyzes nitrogen oxidation reactions, but in addition, we found that ZvFMO did not oxidize the amino group of cysteamine and instead catalyzed the oxidation of the thiol group [5]. Site-directed mutagenesis efforts unveiled residues involved in reducing cofactor selectivity and substrate binding.

2. Experimental procedures

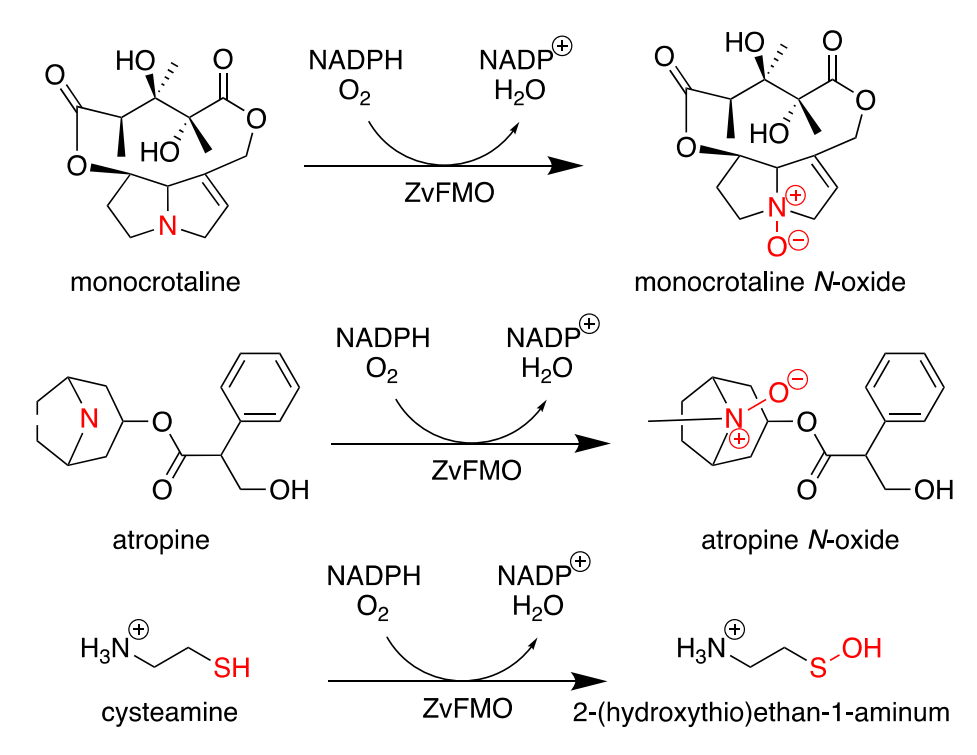
2.1. Materials

Bacterial growth media and buffer reagents were obtained from Fisher Scientific (Pittsburgh, PA). The gene coding for ZvFMO (NCBI Accession Number: FR696373.1) cloned into pET28a was obtained from Genscript Biotech (Piscataway, NJ). *Escherichia coli* BL21(DE3) and One Shot TOP10 chemically competent cells were obtained from Invitrogen (Carlsbad, CA). Glucose oxidase, 1-napthylamine, monocrotaline, and cysteamine were obtained from Sigma-Aldrich (St. Louis, MO). Atropine was obtained from Toronto Research Chemicals (Ontario, Canada). NADPH and NADH were obtained from Research Product International (Mt Prospect, IL). Iodine, sodium thiosulfate, sulfanilic acid, and Ellman's reagent were purchased from Thermo Fisher Scientific (Waltham, MA). For protein purification, a Cytiva Life Sciences (Marlborough, MA) AKTA Start System and HisTrap Fast Flow 5 mL columns were used. The oxygen consumption rate was measured using a Clark-type oxygen electrode system (Hansatech, Norfolk, England). Anaerobic stopped-

flow spectrophotometry was performed with an Applied Photophysics SX20 stopped-flow spectrophotometer (Surrey, UK) housed inside a COY laboratories (Grass Lake, MI) glovebox. Spectral deconvolution was carried out using Applied Photophysics (Surrey, UK) ProKIV software. Site-directed mutagenesis was conducted using the Q5 site-directed mutagenesis kit from New England Biolabs (Ipswich, MA). Primers were synthesized by International DNA Technologies (Coralville, IA).

2.2. Protein expression and purification

The pET28a-ZvFMO plasmid was transformed into chemically competent E. coli BL21 (DE3) cells. Cells were grown in Lysogeny Broth media (10 g tryptone, 10 g NaCl and 5 g yeast extract to 1 L diH₂O) at 37 $^{\circ}\text{C}$ and 250 RPM until an optical density at 600 nm of 0.8 was reached. Expression of ZvFMO was induced with 100 μM of IPTG. The temperature was lowered to 18 $^{\circ}$ C after induction and cells were grown overnight. The cells were harvested by centrifugation and stored at -70 °C. For protein purification, the cell pellet was thawed on ice and resuspended in 5 mL per gram of cell in Buffer A: 50 mM sodium phosphate, 300 mM NaCl, 10 mM imidazole, pH 7.5. The solution was supplemented with 1 mM phenylmethylsulfonyl fluoride (PMSF), 100 μM FAD, 25 μg/mL lysozyme, 10 μg/mL DNAse I, and 10 μg/mL RNAse and was stirred at 4 °C until homogenous. Following this, the lysate was sonicated at 70% amplitude for 15 min, with the pulse on for 5 s and off for 10 s. The lysate was centrifuged at 16,000×g and 4 °C for 45 min to pellet the insoluble material. The supernatant was loaded onto two HisTrap FF, 5 mL columns at 2 mL/min using an AKTA Start system. The columns were washed with 5-column volumes of 10% of Buffer B (50 mM sodium phosphate, 300 mM NaCl, 300 mM imidazole, pH 7.5). ZvFMO was eluted using a gradient of 10% B (30 mM imidazole) to 100% B (300 mM imidazole) over 15 column volumes at 5 mL/min and was collected in 5 mL fractions. ZvFMO eluted between 100 mM and 150 mM imidazole. Fractions were analyzed by SDS-PAGE and fractions with pure protein were pooled. Pooled fractions were concentrated using a 30 kDa molecular weight cutoff filter. The concentrated sample was dialyzed overnight into the storage buffer: 100 mM sodium phosphate, 100 mM NaCl, 1 mM tris(2-carboxyethyl)phosphine (TCEP), 10%



Scheme 1. Reactivity of ZvFMO with A) monocrotaline, B) atropine, and C) cysteamine.

glycerol, pH 7.5. The protein was flash-frozen as droplets and stored at $-70\,^{\circ}$ C. The protein concentration was determined by Bradford assay. The FAD-bound extinction coefficient was measured as previously described to calculate the concentration of FAD-bound protein and flavin incorporation [15,16].

2.3. Oxygen consumption assay

All oxygen consumption assays were performed using an Oxygraph⁺ system from Hansatech Instruments (Norfolk, United Kingdom). Each of the reactions were performed in 1 mL of 50 mM sodium phosphate, 100 mM NaCl, pH 7.5. The reaction was initiated by the addition of enzyme. The steady-state kinetics parameters were determined by varying the concentration of monocrotaline, atropine, cysteamine, NADPH, or NADH in the presence of 1.5 µM ZvFMO. NADPH or NADH concentration was varied (0 μ M-1000 μ M) and monocrotaline was held constant at 1000 µM. When substrate concentration was varied (monocrotaline: 0 μM-1000 μM; atropine: 0-2 mM; cysteamine: 0-20 mM), the NADPH was kept at 200 µM. We also tested ethanolamine and ethylenediamine as potential substrates between 0 and 0.5 M with the same NADPH and enzyme concentrations listed previously. The saturation curves for K215 A/R mutants with NADPH were conducted in the same manner as the wild-type, however up to 2500 µM NADH was required to reach saturation. The activity of N304A was measured similarly to the wildtype, except for atropine, which was saturated to 10 mM. The activity of F383A was measured the same as the wild-type enzyme. Steady-state kinetic parameters and substrate inhibition parameters were obtained by fitting the data to Eq. (1), and Eq. (2) respectively using Kaleidagraph software (Reading, PA). Eq. (1) was used to determine the turnover number (k_{cat}), and Michaelis constant ($K_{\rm M}$). Eq. (2) was used to calculate the inhibition constant (K_{I}).

$$\frac{\nu_0}{[E]} = \frac{k_{cat} \times [S]}{K_M + [S]} \tag{1}$$

$$\frac{\nu_0}{[E]} = \frac{k_{cat} \times [S]}{\left(K_M * \left(1 + \left(\frac{[S]}{K_I}\right)\right)\right)}$$
 (2)

2.4. NADPH oxidation assay

The oxidation of NADPH was measured by monitoring the decrease at 340 nm for 5 min in the presence and absence of substrate. Each of the reactions were performed in 200 μL of 50 mM sodium phosphate, 100 mM NaCl, pH 7.5. The reactions contained 0.4 μM ZvFMO (or mutant enzyme), substrate at a saturating concentration (monocrotaline and atropine =1 mM, cysteamine =20 mM, ethanolamine and ethylenediamine =500 mM), and 100 μM NADPH. Each reaction was initiated with enzyme. The initial rates were recorded and were compared to those of the oxygen consumption assay to determine uncoupling percentage.

2.5. Site-directed mutagenesis

Mutants of ZvFMO were made using the Q5 site-directed mutagenesis kit from New England Biolabs by following the instructions from the manufacturer. Successful mutagenesis was confirmed using Sanger Sequencing conduced at Genomic Sequencing Center at Virginia Tech (Blacksburg, VA). All mutant proteins were purified as described for the wild-type ZvFMO with no modifications.

2.6. Colorimetric product detection assays

Detection for hydroxylated amine product was carried out using the Csáky assay [17]. 120 μ L of a reaction containing 0–0.5 M ethanolamine or ethylenediamine in the presence of 1.5 μ M ZvFMO and 200 μ M

NADPH was reacted at room temperature for 15 min and was quenched with 62.4 μL of 2 N HClO₄. Quenched reactions were centrifuged for 2 min at 16,000×g to remove precipitate. 47 μL of the supernatant or of a hydroxylamine standard (0–300 μM) were transferred to a 96-well plate and 47 μL of 10% (w/v) sodium acetate (prepared in water), 47 μL of 1% (w/v) sulfanilic acid (prepared in 25% glacial acetic acid), and 19 μL 0.5% (w/v) I_2 (prepared in 100% glacial acetic acid) were added. This mixture was incubated at room temperature for 15 min in the dark with shaking at 600 RPM. 19 μL of 0.1 N sodium thiosulfate (prepared in water) and 19 μL of 0.6% (w/v) 1-napthylamine (prepared in 30% glacial acetic acid) were added and the plate was incubated at room temperature for 45 min in the dark with shaking at 600 RPM. The plate was read at 562 nm.

Consumption of cysteamine was monitored using Ellman's reagent [18]. The standard curve was created using 0–2 mM cysteamine and reactions with ZvFMO were conducted using 1.5 μM ZvFMO, 200 μM NADPH, and 1 mM cysteamine. The reactivity of cysteamine with hydrogen peroxide was tested with 200 μM H₂O₂ and 1 mM cysteamine. Reactions were quenched with a 1:1 volume of 2 N HCl after 30 s, 1 min, 2 min, 5 min and 15 min and were then centrifuged for 2 min at 16, 000×g to remove precipitate. 250 μL of sample (or standard) was combined with 50 μL of Ellman's reagent solution (4 mg Ellman's reagent to 1 mL buffer) and 2.5 mL of buffer. This solution was incubated at room temperature for 15 min and the UV–visible spectra were monitored for changes at 412 nm. The amount of cysteamine consumed was determined by using a standard curve. For both product formation assays the buffer utilized was 50 mM sodium phosphate, 100 mM NaCl, pH 7.5.

2.7. Rapid reaction kinetics

The reductive and oxidative-half reactions of ZvFMO were investigated using anaerobic stopped-flow spectroscopy. All concentrations of enzyme, substrate, and reducing cofactors listed in this section are after 1:1 mixing in the stopped-flow. 100 mL of buffers were degassed using four cycles of 28 Hg vacuum pressure (4 min each cycle) and 5 psi argon gas (1 min each cycle) while stirring. The degassed buffers were transferred to the anaerobic chamber. The stopped-flow was deoxygenated overnight with an anaerobic solution of 0.6 μM glucose oxidase and 100 mM glucose in 100 mM sodium acetate, pH 5.0. ZvFMO was made anaerobic using 15 cycles of 28 Hg vacuum pressure (2 s each cycle) and 5 psi argon gas (5 s each cycle). Monocrotaline, NADPH, and NADH were transferred directly to the chamber and resuspended in the anaerobic ZvFMO activity buffer (50 mM sodium phosphate, 100 mM NaCl, pH 7.5). The instrument was blanked with the ZvFMO activity buffer. Flavin reduction was investigated by mixing various concentrations of NADPH or NADH (62.5-2000 μM) with 10 μM ZvFMO in the absence of substrate at room temperature. Absorbance changes at 200-800 nm were recorded. The decreases in absorbance at 455 nm of all experiments unless otherwise noted were fit to Eq. (3) to obtain the observed rate constant ($k_{\rm obs}$). Abs_{nm} is the absorbance at a particular wavelength, A is the amplitude of a phase, t is time, and C is final absorbance at a given wavelength. The WT and K215A mutant were fit to Eq. (4) to account for the slow phase in the reduction. The observed rates as a function of cofactor concentration were fit to Eq. (5) to obtain the maximum rate of flavin reduction ($k_{\rm red}$) and dissociation constant $(K_{\rm D})$ for the reducing cofactor.

$$Abs_{nm} = C + Ae^{-(k_1 \times t)} \tag{3}$$

$$Abs = C + A_1 e^{-(k_1 \times t_1)} + A_2 e^{-(k_2 \times t_2)}$$
(4)

$$k_{obs} = \frac{k_{red} \times [S]}{K_D + [S]} \tag{5}$$

For the flavin oxidation experiments, reduced ZvFMO was prepared by mixing 20 μ M ZvFMO with 20 μ M NAD(P)H in the presence and

absence of 1000 µM monocrotaline prior to mixing in the instrument. Oxygenated buffer was prepared by bubbling 30 cc/min of 100% oxygen into the ZvFMO activity buffer in iced water for 1 h while stirring. This saturated oxygen solution has a concentration of 1.2 mM [19]. The oxygenated buffer was mixed with anaerobic buffer to obtain oxygen concentrations between 50 and 600 µM after mixing. Absorbance changes between 200 and 800 nm were recorded at room temperature. Traces at 390 nm and 455 nm were fit to Eq. (6) to obtain the observed rate constants ($k_{\rm obs}$). In the presence of substrate, traces at 390 nm were fit to Eq. (7) because two phases were observed. All variables are the same as previously defined, except for A_0 , which is the initial absorbance value at a given wavelength. All data fitting was carried out with KaleidaGraph. Oxidation spectra were deconvoluted by performing a global fitting analysis of the spectra with a three-step model, which accounts for the reduced flavin, C4a-(hydro)peroxyflavin, and the fully oxidized flavin using ProKIV software (AppliedPhotophysics, UK). The bimolecular rate constants of the C4a-(hydro)peroxyflavin in the presence and absence of substrate were determined using a linear fit.

$$Abs_{nm} = A(1 - e^{-(k_1 \times t)}) + A_0 \tag{6}$$

$$Abs_{nm} = A_1(1 - e^{-(k_1 \times t_1)}) + A_2(1 - e^{-(k_2 \times t_2)}) + A_0$$
(7)

2.8. Bioinformatic analysis and molecular docking

ZvFMO was aligned to homologs whose functions were previously characterized using MAFFT7 from the European Bioinformatics Institute [20,21]. The alignment was color coded by the Escript3.0 server [22]. Molecular docking was conducted using Autodock Vina and was visualized using PyMOL [23–25].

3. Results and discussion

3.1. Recombinant protein expression and purification

Recombinant ZvFMO was expressed as a fusion to an N-terminal 6x-His tag in *E. coli* BL21 (DE3) cells using an IPTG induction and was purified using Ni²⁺-NTA chromatography (Fig. S1). The protein yield was 7.3 ± 0.3 mg protein/gram of cell. The UV–visible spectrum showed peaks at 380 nm and 455 nm, indicating that ZvFMO purified with FAD bound (Fig. S1). The flavin incorporation was calculated to be 90 ± 4 %.

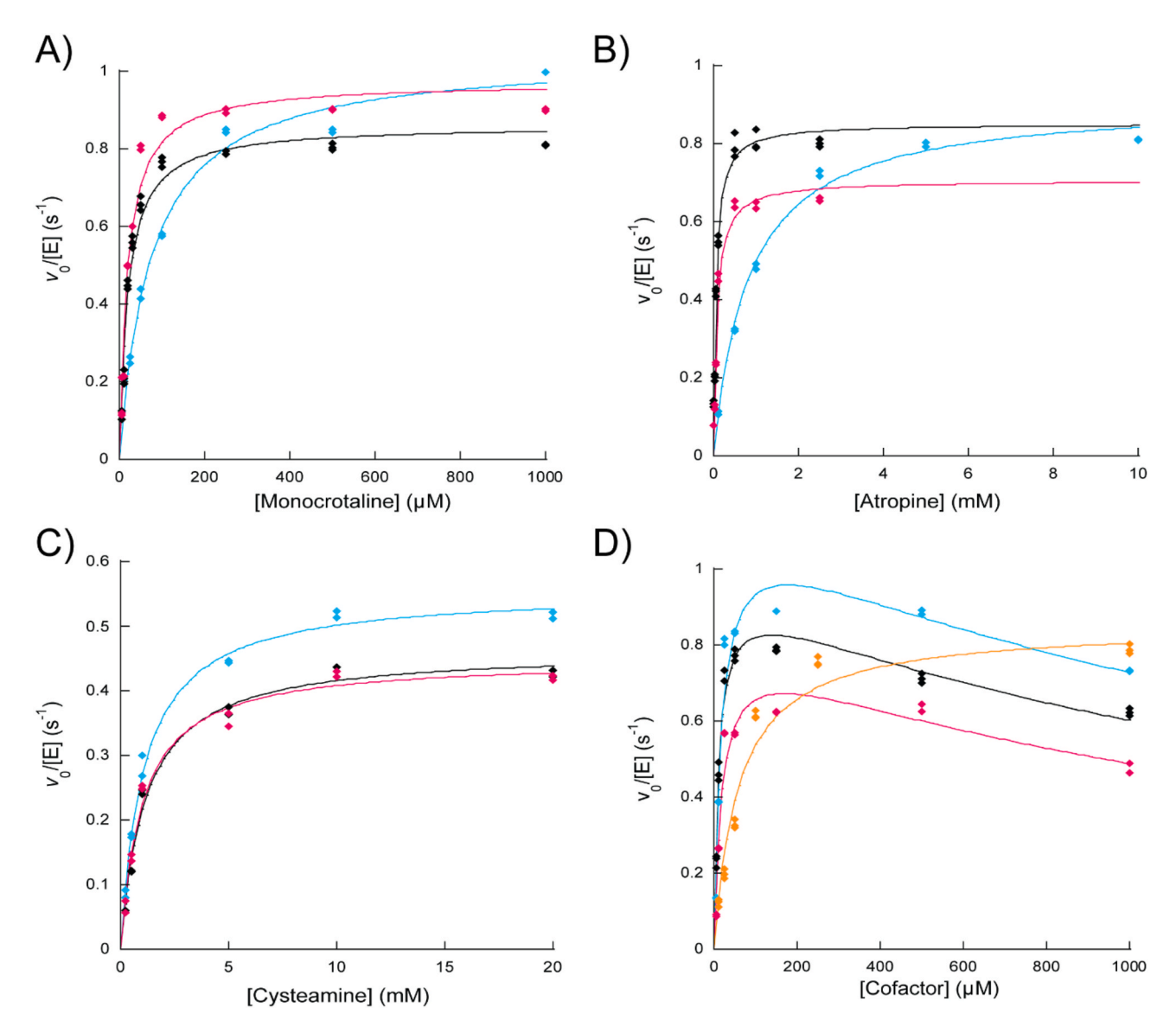


Fig. 1. Steady-state kinetics of ZvFMO. Steady state kinetics of ZvFMO with monocrotaline (A) atropine (B) cysteamine (C), and NADPH and NADH (D). In all panels, the wild-type is in black, N304A is in blue, and F383A is in pink. The orange line in panel D represents the kinetics of wild-type ZvFMO with NADH. All the data were fit to Eq. (1), except the data with NADPH in panel D, which were fit to Eq. (2).

The extinction coefficient of FAD-bound ZvFMO was determined to be $14.7 \pm 0.200 \ mM^{-1} \ cm^{-1}$. All mutant enzymes that will be discussed in greater detail in the bioinformatic analysis section purified very similar to the wild-type enzyme (Fig. S1).

3.2. Steady-state kinetic analysis

The steady-state parameters of ZvFMO with monocrotaline, atropine, cysteamine, ethanolamine, ethylenediamine, NADPH, and NADH were determined by measuring the consumption of oxygen. Experiments with NADPH and NADH showed similar $k_{\rm cat}$ values between the reducing cofactors, with a ~5-fold increase in the $K_{\rm M}$ for NADH compared to NADPH (Fig. 1; Table 1). Saturation with NADPH displayed substrate inhibition, with a $K_{\rm I}$ value of 1700 \pm 300 μ M and was not observed with NADH (Fig. 1; Table 1). This indicates that NADPH is binding to a form of the enzyme-NADPH complex that is not productive for catalysis and has been previously reported to occur in other FMOs [26]. However, we do note that the concentrations of NADPH that we observed inhibition at are likely above the cellular concentrations.

Table 1Steady-state kinetic parameters for ZvFMO.

Steady-state	kinetic parameter	S IOF ZVFMO.					
		Monocrotaline	e				
Enzyme	$k_{\rm cat}~({\rm s}^{-1})$	$K_{\rm M}~(\mu{ m M})$	$K_{\rm I}~(\mu{ m M})$	$k_{\text{cat}}/K_{\text{M}}$ $(\text{M}^{-1}\cdot\text{s}^{-1})$			
WT	0.88 ± 0.020	14 ± 2.0	N.D.	$42,000 \pm 290$			
N304A	1.1 ± 0.010	80 ± 3	N.D.	$14,\!000\pm510$			
F383A	0.97 ± 0.030	19 ± 2.4	N.D.	$51,\!000\pm560$			
Enzyme	$k_{\rm cat}$ (s ⁻¹)	Atropine K _M (μM)	<i>K</i> _I (μM)	$k_{\text{cat}}/K_{\text{M}}$ $(\text{M}^{-1}\cdot\text{s}^{-1})$			
WT	0.87 ± 0.020	61 ± 4.3	N.D.	$14,\!000\pm780$			
N304A	0.91 ± 0.020	830 ± 67	N.D.	1100 ± 65			
F383A	0.71 ± 0.020	78 ± 9.0	N.D.	9000 ± 100			
Cysteamine							
Enzyme	$k_{\rm cat}~({\rm s}^{-1})$	$K_{\rm M}$ (μ M)	$K_{\rm I}~(\mu{ m M})$	$\begin{array}{c} k_{\rm cat}/K_{\rm M} \\ ({\rm M}^{-1}{\cdot}{\rm s}^{-1}) \end{array}$			
WT	0.46 ± 0.010	1100 ± 120	N.D.	400 ± 30			
N304A	0.56 ± 0.010	1100 ± 76	N.D.	520 ± 33			
F383A	0.44 ± 0.010	1000 ± 100	N.D.	440 ± 44			
		NADPH					
Enzyme	$k_{\rm cat}~({\rm s}^{-1})$	$K_{\rm M}$ (μ M)	$K_{\rm I}$ ($\mu { m M}$)	$\begin{array}{c} k_{\rm cat}/K_{\rm M} \\ ({\rm M}^{-1}\cdot{\rm s}^{-1}) \end{array}$			
WT	0.96 ± 0.040	11 ± 1.3	$\overline{1700\pm280}$	87,000 ± 790			
N304A	1.2 ± 0.070	26 ± 4.0	1600 ± 350	$45,000 \pm 370$			
F383A	0.82 \pm	19 ± 4.9	1500 ± 470	$44,000 \pm 780$			
K215R	$\begin{array}{c} \textbf{0.080} \\ \textbf{0.77} \ \pm \end{array}$	$\textbf{8.4} \pm \textbf{1.1}$	4600 ±	$91,\!000\pm860$			
K215A	$0.030 \\ 1.0 \pm 0.020$	63 ± 4.1	1600 N.D.	$17,000 \pm 190$			
	110 ± 01020			17,000 ± 130			
Enzyme	$k_{\rm cat}~({\rm s}^{-1})$	NADH $K_{\rm M}$ (μ M)	$K_{\rm I}$ ($\mu { m M}$)	$k_{\text{cat}}/K_{\text{M}}$ $(M^{-1}\cdot s^{-1})$			
WT	0.86 ± 0.020	59 ± 6.4	N.D.	14,000 ± 1300			
K215R	0.79 ± 0.020	49 ± 5.8	N.D.	$16,\!000\pm190$			
K215A	0.65 ± 0.020	88 ± 9.0	N.D.	7000 ± 70			

Conditions: 50 mM sodium phosphate, 100 mM NaCl, pH 7.5. Error values were obtained from the data fitting analysis. When reducing cofactor was varied, monocrotaline was the fixed substrate and when substrates were varied, NADPH was fixed. Ethanolanime and ethylenediamine were tested but only produced hydrogen peroxide (see Figure S2).

ZvFMO has similar $k_{\rm cat}$ values for monocrotaline and atropine, which both have tertiary nitrogen that is oxidized (Fig. 1; Table 1). The $K_{\rm M}$ value for monocrotaline is \sim 3-fold lower than that of atropine, which also results in a 3-fold increase in the $k_{\rm cat}/K_{\rm M}$ (Fig. 1; Table 1). We also tested the reactivity of smaller substrates with primary amines such as cysteamine. Cysteamine had a lower $k_{\rm cat}$ value than the tertiary nitrogen-containing substrates and a much higher $K_{\rm M}$ value (Fig. 1 & Table 1). This suggests that ZvFMO binds large, hydrophobic substrates and reacts most optimally with tertiary nitrogen atoms compared to small substrates that contain primary amino and/or sulfur groups.

One limitation of this approach is that the oxygen consumption assay cannot distinguish between the production of hydrogen peroxide and product oxygenation. While FMOs typically couple oxygen activation and substrate hydroxylation, in cases where the substrate is not present or is not optimal, an unproductive uncoupling reaction can occur, which produces hydrogen peroxide [27–30]. To determine how uncoupled ZvFMO is with its substrates, we monitored the oxidation of NADPH spectroscopically in the absence and in the presence of each substrate and compared the rates to those obtained from the oxygen consumption assay under the same conditions.

We found that ZvFMO was highly uncoupled regardless of the substrate (Table S1). With monocrotaline, the enzyme is $39 \pm 4\%$ uncoupled and was even more uncoupled at 60 \pm 2 % with atropine. Cysteamine was also very uncoupled at 71 \pm 5%. Conducting this experiment with ethanolamine and ethylenediamine demonstrated rates very close to the rate in the absence of substrate, indicating no product was formed (100% uncoupled). These findings were verified by detecting for hydroxylamine products using an iodine oxidation assay, where we were unable to detect any hydroxylated amine product for either substrate (Fig. S2). We determined that the iodine oxidation assay was not suitable in the presence of thiol groups to study reactivity with cysteamine, because the thiol reduced the iodine, and did not form a diazonium with sulfanilic acid, an essential step for color formation (not shown) [17]. Therefore, we monitored the oxidation of free thiols using Ellman's reagent to determine if ZvFMO was acting on the sulfur atom of cysteamine. These experiments showed that ZvFMO oxidized the thiol of cysteamine at a rate of 4.2 \times 10⁻³ \pm 1.0 \times 10⁻⁴ μ M/s⁻¹ (Fig. S3). However, ZvFMO is highly uncoupled with cysteamine and mainly produces hydrogen peroxide, which can act with free thiol groups to form sulfenic acid, sulfinic acid, and sulfonic acid [31,32]. Thus, we performed the same assay with hydrogen peroxide without enzyme and recorded a cysteamine oxidative rate of 1.2 \times 10⁻³ \pm 0.6 \times 10⁻⁴ μ M/s⁻¹, which is 3-fold slower than with enzyme (Fig. S3). This indicates that sulfur oxidation is coupled to oxygen activation by ZvFMO and is not oxidized solely by the hydrogen peroxide produced as the reaction byproduct.

3.3. Rapid-reaction kinetic analysis

Analyses of the reductive and oxidation-half reactions were performed using anaerobic stopped-flow spectrophotometry. Flavin reduction was monitored by monitoring the bleaching of the oxidized flavin at 455 nm. Flavin reduction was bi-phasic with NADPH (Fig. 2). We attribute the second phase to be associated with a charge-transfer complex between the reduced flavin and NADP+, which agrees with other reports [10,26]. The rates of the formation of the charge-transfer complex ($\sim 0.3 \text{ s}^{-1}$) were very similar across all concentrations of NADPH. The reduction with NADH occurred in a single-phase and was 2-fold slower than with NADPH (Fig. 2& S4; Table 2). The K_D value for NADH is ~31-fold higher than with NADPH (precise value could not be determined because much lower enzyme concentration was needed, and data collection became problematic) (Fig. 2 & S4; Table 2). Together, these experiments demonstrate that ZvFMO binds NADPH with greater affinity than NADH and prefers to utilize NADPH over NADH as the reducing cofactor, which agrees with many previous works on FMOs [10,26,33,34].

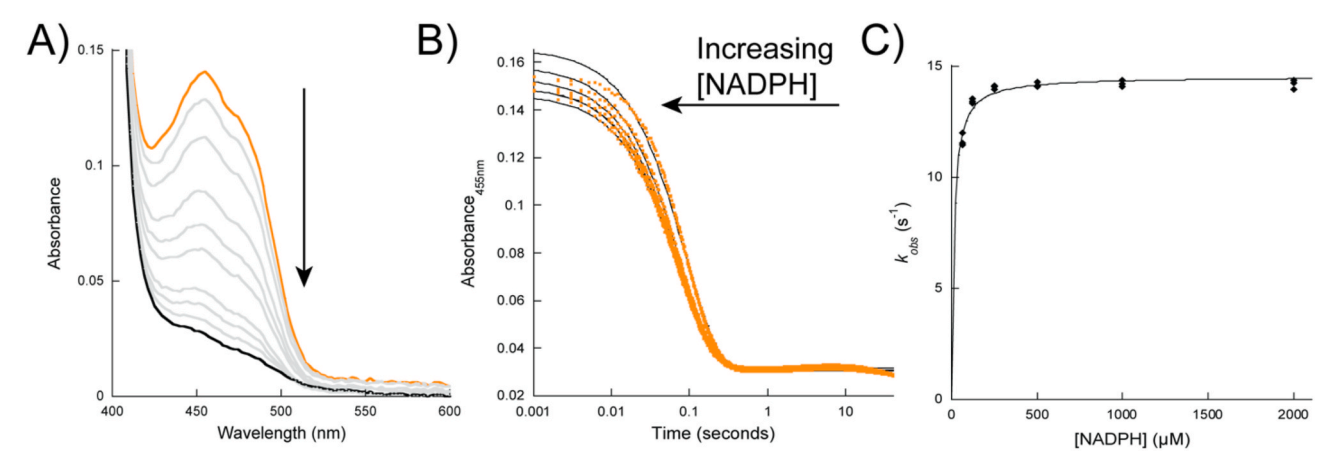


Fig. 2. Reductive-half reaction of ZvFMO WT with NADPH. A) Representative reduction the spectra changes upon reaction with 2 mM NADPH over 60 s. The reduced flavin is indicated by the black line and the oxidized flavin is shown in orange. B) Representative traces for each concentration of NADPH. The solid lines are fit to Eq. (4). C) Observed rates of reduction as a function of [NADPH], the line is a fit to Eq. (5).

Table 2
Reductive-half reaction parameters for ZvFMO WT and K215 R/A mutants.

Enzyme	Cofactor	$k_{\rm red}~({\rm s}^{-1})$	$K_{\rm D}$ (μM)	$k_{\rm red}/K_{\rm D}~({ m M}^{-1}{ m \cdot s}^{-1})$
WT	NADPH	14.5 ± 0.200	≤14	1,000,000 ± 90,000
WT	NADH	8.00 ± 0.175	440 ± 25.8	$180,000 \pm 7900$
K215R	NADPH	14.6 ± 0.100	≤ 1	$10,\!000,\!000 \pm 5,\!000,\!000$
K215A	NADPH	17.9 ± 0.580	650 ± 50	$27,000 \pm 1400$

Conditions: 50 mM sodium phosphate, 100 mM NaCl, pH 7.5. Error values were obtained from the data fitting analysis.

Flavin oxidation was monitored following the changes in absorbance during the reaction of the reduced enzyme with oxygen. During this process, a peak with an absorption maxima at 390 nm forms very fast in the presence or absence of substrate. Spectral deconvolution showed a spectrum with a peak at 390 nm that closely resembled the C4a-(hydro) peroxyflavin (Fig. 3 & S5; Table 3) [14]. In the presence of substrate, the intermediate formation was a biphasic process (Fig. S5). At 300 µM oxygen, the first phase was determined to occur at $25 \pm 0.40 \,\mathrm{s}^{-1}$, while the second phase was $2.4 \pm 0.04 \text{ s}^{-1}$ (Table 3). We assign the second phase to the unproductive decay of the C4a-(hydro)peroxyflavin, as it was determined that the reaction is uncoupled with all substrates tested. We determined that the bimolecular rate constant of C4a-(hydro)peroxyflavin formation is ~1.6 fold faster in the presence of substrate than in the absence (Table 3). The rate of flavin oxidation in the absence of substrate (k_{H2O2}) represents the decay of the C4a-(hydro)peroxyflavin to hydrogen peroxide (since chemistry is not occurring). This occurs \sim 330-fold slower than the rate of flavin oxidation (k_{OX}) in the presence of monocrotaline and does not fully complete even after more than 16 min of monitoring the reaction at room temperature (Fig. 3 & S5; Table 3). These findings are consistent with the stabilization of the C4a-(hydro)peroxyflavin until substrate binds in a productive conformation for catalysis, which is also referred to as the "cocked-gun" mechanism [12,35,36]. Flavin oxidation in the presence of monocrotaline closely resembled the k_{cat} value obtained from steady-state experiments, which suggests that flavin oxidation and/or NADP+/product release are the rate-limiting steps of the reaction (Tables 1 and 3).

3.4. Bioinformatic analysis and mutagenesis

Multiple sequence alignment with homologs to ZvFMO and molecular docking were used to identify residues that could be involved in substrate binding and cofactor selectivity. Previous work proposed that the movement of an alpha helix ($\alpha 8$) near the active site is responsible for accommodating the large bulky substrates of ZvFMO (Fig. 4A and S6)

[9]. Most of the residues that face towards the active site in this helix are small and hydrophobic amino acids such as valine and leucine. One residue in this helix, F383, was previously proposed to have a role in binding the substrates of ZvFMO [9]. This residue is highly conserved in FMOs with similar reactivity to ZvFMO and was mutated to alanine to probe its potential role in substrate selectivity (Fig. S6). The steady-state kinetic analysis of F383A showed that all values for monocrotaline, atropine, cysteamine, and NADPH were very similar to the wild-type enzyme (Fig. 1; Table 1). Docking monocrotaline, atropine, and cysteamine into the active site was consistent with these findings, as each of the substrates were at least 4.7 Å from F383 and are too far to interact. The docking also revealed a loop in the predicted substrate binding site, which contains an asparagine (N304) that is capable of hydrogen bonding with substrates of ZvFMO and is unique to ZvFMO (Fig. 4B and S6). N304 is in close enough proximity to form a hydrogen bond with monocrotaline and atropine, but not cysteamine (Fig. 4). The amino group of cysteamine could hydrogen bond with a hydroxyl group of the NADP⁺ ribose and does not appear to have interactions with residues in the active site (Fig. 4). To test the possibility that N304 interacts with monocrotaline and atropine, the residue was mutated to alanine. Steady-state kinetic analysis of N304A showed a ~6-fold increase in the $K_{\rm M}$ value for monocrotaline and a ~13-fold increase in the $K_{\rm M}$ value for atropine with little change in the k_{cat} values (Fig. 1; Table 1). As predicted by the docking model, the k_{cat} and K_{M} values with cysteamine were not impacted by the mutation (Fig. 1; Table 1). Neither of the mutations to F383 or N304 impacted uncoupling with any of the substrates compared to the wild-type enzyme. The kinetic parameters for NADPH did not change for N304A, indicating that no major structural changes were introduced by the mutation (Fig. 1; Table 1).

ZvFMO has a lysine residue (K215) that is hydrogen bonding with the 2'-phosphate of NADP⁺, which is a histidine residue in homologous enzymes (Figs. S6 and 7). We hypothesized that this lysine is responsible for conferring cofactor selectivity in ZvFMO. We mutated K215 to alanine to disrupt the interaction with NADP⁺ and to arginine to increase the potential number of interactions from one to two hydrogen bonds with NADP $^+$. Steady-kinetic analysis showed that the k_{cat} values were unchanged for both mutants (Table 1; Fig. S8). Neither of the mutations impacted the uncoupling compared to the wild-type enzyme. The K215R mutant had very little change to the $K_{\rm M}$ value with NADPH or NADH, whereas there was a \sim 6-fold increase in the $K_{\rm M}$ for NADPH with the K215A mutant with a similar $K_{\rm M}$ value for NADH to the wildtype (Table 1; Fig. S8). We aimed to determine if any of these differences would influence the rate of flavin reduction and the KD for NADPH. For the K215R mutant, there was no change to the k_{red} , but there was a 14-fold decrease in the K_D for NADPH compared to the wild-

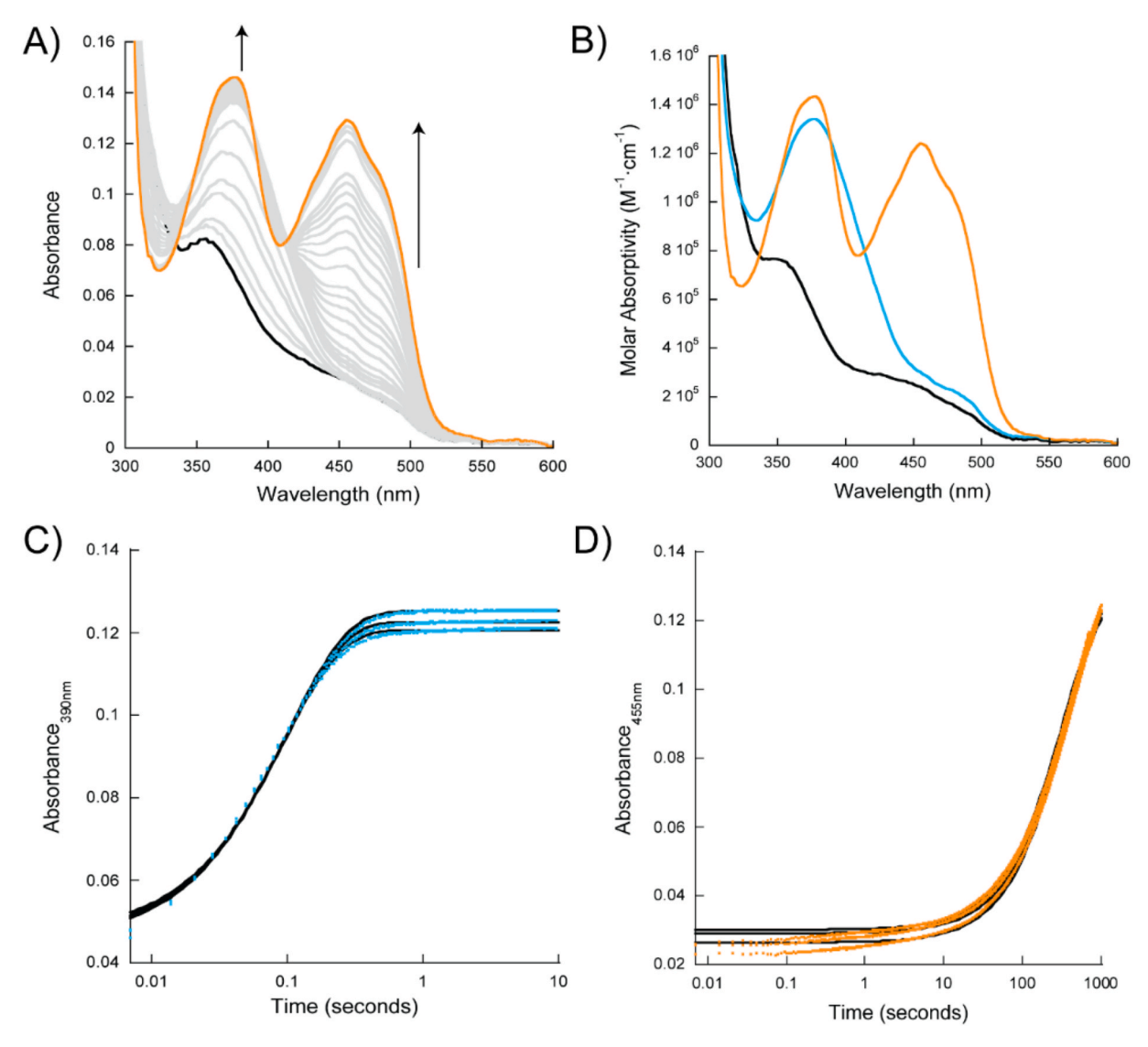


Fig. 3. Oxidation of ZvFMO WT in the absence of substrate at 300 μM oxygen. A) Oxidation spectra over 1000 s at 300 μM oxygen. The starting spectrum is in black, and the final spectrum is in orange. B) Deconvolution of the oxidation spectra. The reduced flavin is shown in black, the C4a-(hydro)peroxyflavin is shown in blue, and the oxidized flavin is in orange. C) Experimental replicate traces at 390 nm monitoring the formation of the C4a-(hydro)peroxyflavin. The data were fit to Eq. (6). D) Experimental replicate traces at 455 nm, monitoring flavin oxidation. The black lines are fits to. Eq. (6). All traces shown were obtained at 300 μM oxygen.

Table 3 Oxidative-half reaction parameters for ZvFMO.

Condition	$k_{\text{OOH}} (M^{-1} \cdot s^{-1})$	$k_{\rm OX}~({\rm s}^{-1})$
- Monocrotaline + Monocrotaline	$\begin{array}{c} 3.5\times10^{4}\pm1.6\times10^{3} \\ 5.6\times10^{4}\pm3.0\times10^{3} \end{array}$	$\begin{array}{c} 0.003 \pm 0.001 \\ 1.0 \pm 0.10 \end{array}$

Conditions: 50 mM sodium phosphate, 100 mM NaCl, pH 7.5, 300 μM $O_2.$ Errors are the standard deviation of three replicates.

type (Table 2; Fig. S9). The same experiment with K215A showed little change to the $k_{\rm red}$, but also a 46-fold increase in the $K_{\rm D}$ for NADPH. Reduction of K215A also showed a slow phase that was not dependent on the NADPH concentration and accounted for ~8% of the total amplitude change (Table 2; Fig. S9). All these results suggest that K215 is responsible for conferring cofactor selectivity and that mutagenesis to an arginine does increase the selectivity for NADPH over NADH.

4. Conclusions

The mechanisms of microbial FMOs have been very well

characterized and have not been described for FMOs from insects due to a lack of soluble and active recombinant proteins [3,8,37,38]. Other FMOs from insects contain an N-terminal signaling peptide that localizes the enzymes to the hemolymph of insects where the enzymes are soluble, but ZvFMO lacks the signaling peptide and is soluble in the fat body of the insect (Fig. S6) [3,5,6]. Truncation of the signaling peptide in a ZvFMO homolog from *Grammia geneura* did generate small amounts of active and soluble protein [6]. The natural absence of the signaling peptide in ZvFMO presented a unique opportunity to explore the mechanism of the enzyme without the additional hurdle of obtaining soluble protein or the need for an insect-driven expression system. ZvFMO represents the first insect FMO to have the structure solved and now we propose the kinetic and chemical mechanism (Fig. 5) [9].

ZvFMO has the structural features that classify the enzyme to belong to the class B of the FMO family and the class B subgroup of a flavin-containing monooxygenase [8]. The structure of ZvFMO features the hallmarks of two nucleotide binding Rossman-folds—one to bind FAD and one to bind NADP $^+$ [8,9]. The structure of ZvFMO closely resembles that of another well-characterized class B FMO, AsFMO from the plant Allium sativum (RMSD = 1.48 Å; 32% identity) [26]. Enzymes in class B

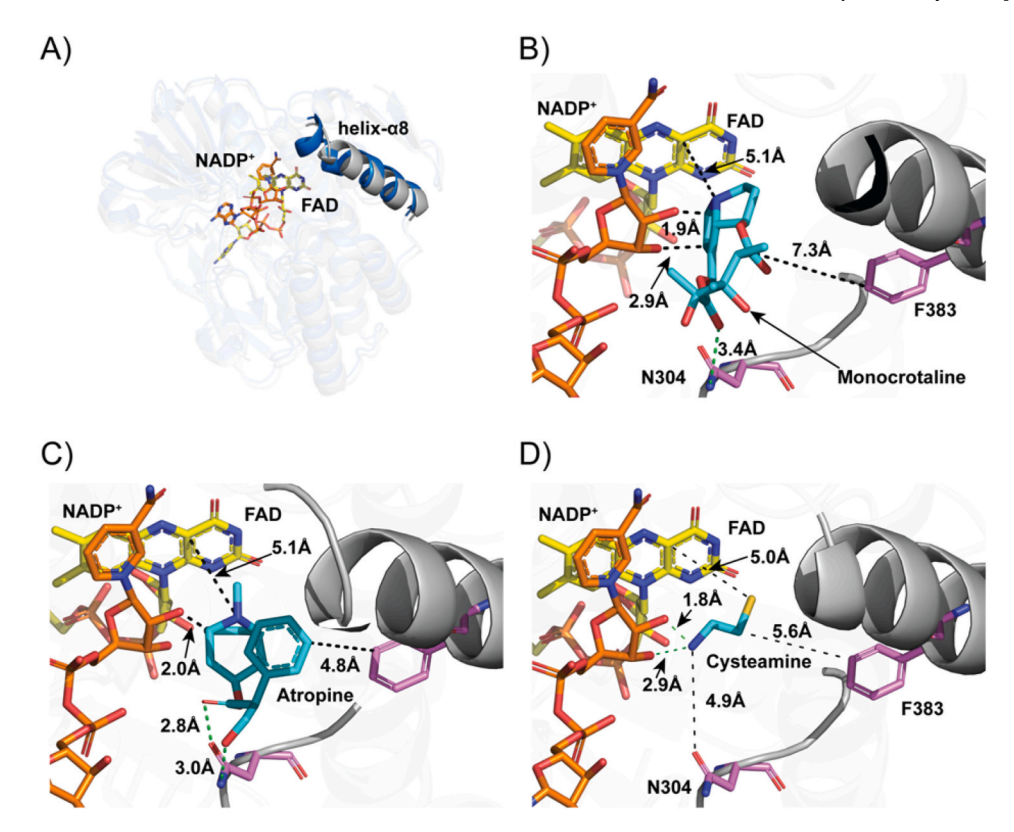


Fig. 4. Molecular docking of substrates into the predicted substrate binding pocket of ZvFMO. A) Movement of a helix close to the substrate binding pocket when NADP⁺ is present (gray) versus absent (blue). Binding pocket of B) monocrotaline, C) atropine, and D) cysteamine. In all panels: the FAD is colored in yellow, and NADP⁺ is colored in orange, substrates are colored blue, and residues of interest are colored pink. All black lines show distances and green lines are indicative of potential interactions. PDB ID: 5NMX; chain A.

utilize the "bold" mechanism of flavin reduction where the substrate does not need to be bound to reduce the enzyme [34,39]. This is in contrary to the "cautious" mechanism that is employed by Class A FMOs in which the substrate must bind to move the flavin into the optimal position for reduction (enhancing reduction rates up to 10⁵) and is utilized to prevent the wasteful production of hydrogen peroxide [11,14, 40]. The reaction of ZvFMO starts with high affinity binding of NADPH and fast hydride transfer that does not require the presence of substrate, supporting the "bold" mechanism (Fig. 2; 5A.1&2, and Table 2). It has been proposed that other class B FMOs prevent hydrogen peroxide production by stabilizing the C4a-(hydro)peroxyflavin and have attributed this stabilization to NADP+ remaining bound throughout the catalytic cycle [13]. Our data demonstrates a very stable C4a-(hydro) peroxyflavin in the absence of substrate and agrees with previously proposed mechanisms of class B FMOs (Figs. 3 and 5A.3 and Table 3) [8, 14,26]. Following intermediate formation, the substrate binds and is oxidized via a nucleophilic attack from the nitrogen (or sulfur) atom to the electrophilic C4a-(hydro)peroxyflavin (Fig. 5A.4&5). We propose that following hydroxylation, the expected low pKa value of the intermediate will lead to a non-enzymatic deprotonation to the N-oxide form (Fig. 5B). Upon flavin oxidation and release of NADP⁺ and product, the oxidized ZvFMO is regenerated, and a new cycle can start (Fig. 5A.6). Our results demonstrated that ZvFMO is very uncoupled, suggesting that substrate binding is not always optimal and can acquire different conformations, where some lead to destabilization of the C4a-(hydro)peroxyflavin (Fig. 5A.7)

Flavin-containing monooxygenases have been shown to catalyze the oxidation of soft nucleophiles such as nitrogen or sulfur atoms on xenobiotic substrates and have wide substrate selectivity to accommodate various xenobiotics [14]. Our steady-state and product formation characterization demonstrate that ZvFMO can oxidize nitrogen or sulfur atoms on a variety of substrates (Fig. 1; S2; S3 and Table 1). Previous

reports showed that FMOs from insects who are generalist feeders such as Z. variegatus and G. geneura have very broad substrate selectivity whereas FMOs from a specialist feeder such as Tyria jacobaeae are much more selective [5,6]. These findings indicate that the FMO active site evolves to accommodate the plant-secreted alkaloids that are specific to the diet of the insect with low conservation across all insect FMOs. This agrees with our findings that showed a role for N304 substrate binding in ZvFMO and is not conserved in other insect FMOs (Fig. 1 and Table 1). F383 was previously proposed to play a role in substrate binding, but our data does not support that proposal (Fig. 1 and Table 1) [9]. We also explored the cofactor selectivity of an insect FMO, and we found that ZvFMO prefers NADPH over NADH, which agrees with studies of other flavin-dependent monooxygenases [10,26,33,34]. We determined that the cofactor selectivity is conferred by K215 (Figs. S8 and 9 and Tables 1 and 2). This residue was not conserved in other FMOs and is replaced with a histidine and could carry out the same function as a lysine if protonated (Fig. S5).

The extensive characterization of ZvFMO in this work represents the first of its kind on an FMO from insects. Our proposed kinetic and chemical mechanisms are in strong agreement of other well-studied FMOs. The site-directed mutagenesis and molecular docking efforts revealed information about the active site of ZvFMO, which was necessary in the absence of a substrate-bound crystal structure. ZvFMO is proposed to confer the resistance of plant-secreted alkaloid compounds to the insect food crop pest *Z. varigetus*, making the enzyme an attractive insecticide target. In combination with the crystal structure, the work presented here will be of great benefit for future studies of related enzyme and for drug discovery efforts.

Accession codes

ZvFMO (or ZvPNO) NCBI Nucleotide Accession Number:

Fig. 5. Proposed kinetic and chemical mechanism of ZvFMO. A) In the reductive-half reaction, NADPH binds (step 1) and transfers a hydride from the c4 of the nicotinamide ring to the N5 of the flavin, reducing it (step 2). In the oxidative-half reaction, the reduced flavin reacts with molecular oxygen to form the C4a-(hydro) peroxyflavin (step 3). Upon binding of the substrate (step 4), the C4a-(hydro)peroxyflavin will reaction with the substrate forming the oxygenated product and the C4a-hydroxyflavin (step 5). Lastly, the flavin is dehydrated back to the oxidized form and product/NADP⁺ are released to restart the cycle (step 6). B) The tertiary nitrogen atom of monocrotaline performs a nucleophilic attack on the C4a-(hydro)peroxyflavin, generating monocrotaline *N*-hydroxide. Protonation of the flavin C4a oxygen will form the C4a-hydroxyflavin and deprotonation of monocrotaline *N*-hydroxide will occur rapidly, monocrotaline *N*-oxide. It is likely that each substrate would react in this manner.

FR696373.1 and Protein Accession Number: CBX26645.1.

Funding sources

This research was supported by National Science Foundation grant CHE-2003658.

Notes

The authors declare no competing financial interest.

CRediT authorship contribution statement

Sydney B. Johnson: Writing – review & editing, Writing – original draft, Data curation, Conceptualization. **Kathryn Paasch:** Conceptualization. **Starlina Shepard:** Data curation. **Pablo Sobrado:** Writing – review & editing, Writing – original draft, Supervision, Project administration, Funding acquisition, Formal analysis, Conceptualization.

Acknowledgments

This work was supported by the U.S. National Science Foundation under the grant CHE 2003658. Further financial support was provided by the College of Agriculture and Life Sciences and the Department of Biochemistry under the Graduate Teaching Scholars program at Virginia Tech.

Appendix A. Supplementary data

Supplementary data to this article can be found online at $https://doi.\ org/10.1016/j.abb.2024.109949.$

Abbreviations

FMO flavin-dependent monooxygenase

ZvFMO Zonocerus variegatus flavin-dependent monooxygenase

References

 S. Kekeunou, S. Weise, J. Messi, M. Tamò, Farmers' perception on the importance of variegated grasshopper (Zonocerus variegatus (L.)) in the agricultural

- production systems of the humid forest zone of Southern Cameroon, J. Ethnobiol. Ethnomed. 2 (1) (2006) 17, https://doi.org/10.1186/1746-4269-2-17.
- [2] W. African Crop Science Society, Control of the Variegated Grasshopper Zonocerus Variegatus (L.) on Cassava, African Crop Science Society, 1994.
- [3] C. Naumann, T. Hartmann, D. Ober, Evolutionary recruitment of a flavin-dependent monooxygenase for the detoxification of host plant-acquired pyrrolizidine alkaloids in the alkaloid-defended arctiid moth *Tyria jacobaeae*, Proc. Natl. Acad. Sci. USA 99 (9) (2002) 6085–6090, https://doi.org/10.1073/pnag-082674409
- [4] E. Roeder, Medicinal plants in Europe containing pyrrolizidine alkaloids, Pharmazie 50 (2) (1995) 83–98.
- [5] L. Wang, T. Beuerle, J. Timbilla, D. Ober, Independent recruitment of a flavin-dependent monooxygenase for safe accumulation of sequestered pyrrolizidine alkaloids in grasshoppers and moths, -e31796, PLoS One 7 (2) (2012) e31796, https://doi.org/10.1371/journal.pone.0031796.
- [6] S. Sehlmeyer, L. Wang, D. Langel, D.G. Heckel, H. Mohagheghi, G. Petschenka, D. Ober, Flavin-dependent monooxygenases as a detoxification mechanism in insects: new insights from the arctiids (lepidoptera), -e10435, PLoS One 5 (5) (2010) e10435, https://doi.org/10.1371/journal.pone.0010435.
- [7] E. Romero, J.R. Gómez Castellanos, G. Gadda, M.W. Fraaije, A. Mattevi, Same substrate, many reactions: oxygen activation in flavoenzymes, Chem. Rev. 118 (4) (2018) 1742–1769, https://doi.org/10.1021/acs.chemrev.7b00650.
- [8] M.M. Huijbers, S. Montersino, A.H. Westphal, D. Tischler, W.J. van Berkel, Flavin dependent monooxygenases, Arch. Biochem. Biophys. 544 (2014) 2–17, https://doi.org/10.1016/j.abb.2013.12.005.
- [9] C. Kubitza, A. Faust, M. Gutt, L. Gäth, D. Ober, A.J. Scheidig, Crystal structure of pyrrolizidine alkaloid N-oxygenase from the grasshopper Zonocerus variegatus, Acta Crystallogr. D Struct. Biol. 74 (Pt 5) (2018) 422–432, https://doi.org/ 10.1107/s2059798318003510.
- [10] W.J.H. van Berkel, N.M. Kamerbeek, M.W. Fraaije, Flavoprotein monooxygenases, a diverse class of oxidative biocatalysts, J. Biotechnol. 124 (4) (2006) 670–689, https://doi.org/10.1016/j.jbiotec.2006.03.044.
- [11] M. Husain, V. Massey, Kinetic studies on the reaction of p-hydroxybenzoate hydroxylase. Agreement of steady state and rapid reaction data, J. Biol. Chem. 254 (14) (1979) 6657–6666, https://doi.org/10.1016/S0021-9258(18)50419-1.
- [12] R. Robinson, S. Badieyan, P. Sobrado, C4a-hydroperoxyflavin formation in N-hydroxylating flavin monoxygenases is mediated by the 2'-OH of the nicotinamide ribose of NADP, Biochemistry 52 (51) (2013) 9089–9091, https://doi.org/10.1021/bi4014903.
- [13] C. Shirey, S. Badieyan, P. Sobrado, Role of ser-257 in the sliding mechanism of NADP(H) in the reaction catalyzed by the Aspergillus fumigatus flavin-dependent ornithine N5-monooxygenase SidA, J. Biol. Chem. 288 (45) (2013) 32440–32448, https://doi.org/10.1074/jbc.M113.487181.
- [14] D.P. Ballou, B. Entsch, 1 the reaction mechanisms of Groups A and B flavoprotein monooxygenases, in: H. Russ, M. Susan, P. Bruce (Eds.), Volume 2 Complex Flavoproteins, Dehydrogenases and Physical Methods, De Gruyter, 2013, pp. 1–28.
- [15] M. Oppenheimer, M.B. Poulin, T.L. Lowary, R.F. Helm, P. Sobrado, Characterization of recombinant UDP-galactopyranose mutase from Aspergillus fumigatus, Arch. Biochem. Biophys. 502 (1) (2010) 31–38, https://doi.org/ 10.1016/j.abb.2010.06.035.
- [16] K. Chapman, A. Reid, Methods in Molecular Biology: Flavoprotein Protocols, vol. 131, Springer, Totowa, NJ, 1999, p. 5.
- [17] T.Z. Csáky, O. Hassel, T. Rosenberg, S. Lång, E. Turunen, A. Tuhkanen, On the estimation of bound hydroxylamine in biological materials, Acta Chem. Scand. 2 (1948) 450-454
- [18] G.L. Ellman, Tissue sulfhydryl groups, Arch. Biochem. Biophys. 82 (1) (1959) 70–77, https://doi.org/10.1016/0003-9861(59)90090-6.
- [19] H. Valentino, P. Sobrado, Performing anaerobic stopped-flow spectrophotometry inside of an anaerobic chamber, Methods Enzymol. 620 (2019) 51–88, https://doi. org/10.1016/bs.mie.2019.03.006.
- [20] K. Katoh, D.M. Standley, MAFFT multiple sequence alignment software version 7: improvements in performance and usability, Mol. Biol. Evol. 30 (4) (2013) 772–780, https://doi.org/10.1093/molbev/mst010.
- [21] F. Madeira, M. Pearce, A.R.N. Tivey, P. Basutkar, J. Lee, O. Edbali, N. Madhusoodanan, A. Kolesnikov, R. Lopez, Search and sequence analysis tools services from EMBL-EBI in 2022, Nucleic Acids Res. 50 (W1) (2022) W276–W279, https://doi.org/10.1093/nar/gkac240.

- [22] X. Robert, P. Gouet, Deciphering key features in protein structures with the new ENDscript server, Nucleic Acids Res. 42 (W1) (2014) W320–W324, https://doi. org/10.1093/nar/gku316.
- [23] O. Trott, A.J. Olson, AutoDock Vina: improving the speed and accuracy of docking with a new scoring function, efficient optimization, and multithreading, J. Comput. Chem. 31 (2) (2010) 455–461, https://doi.org/10.1002/jcc.21334.
- [24] J. Eberhardt, D. Santos-Martins, A.F. Tillack, S. Forli, AutoDock Vina 1.2.0: new docking methods, expanded force field, and Python bindings, J. Chem. Inf. Model. 61 (8) (2021) 3891–3898, https://doi.org/10.1021/acs.jcim.1c00203.
- [25] L.L.C. Schrodinger, The PyMOL Molecular Graphics System, 2015. Version 2.5.
- [26] H. Valentino, A.C. Campbell, J.P. Schuermann, N. Sultana, H.G. Nam, S. LeBlanc, J. J. Tanner, P. Sobrado, Structure and function of a flavin-dependent S-monooxygenase from garlic (Allium sativum), J. Biol. Chem. 295 (32) (2020) 11042–11055, https://doi.org/10.1074/jbc.RA120.014484.
- [27] S. Franceschini, M. Fedkenheuer, N.J. Vogelaar, H.H. Robinson, P. Sobrado, A. Mattevi, Structural insight into the mechanism of oxygen activation and substrate selectivity of flavin-dependent N-hydroxylating monooxygenases, Biochemistry 51 (36) (2012) 7043–7045, https://doi.org/10.1021/bi301072w.
- [28] C. Binda, R.M. Robinson, J.S. Martin del Campo, N.D. Keul, P.J. Rodriguez, H. H. Robinson, A. Mattevi, P. Sobrado, An unprecedented NADPH domain conformation in lysine monooxygenase NbtG provides insights into uncoupling of oxygen consumption from substrate hydroxylation, J. Biol. Chem. 290 (20) (2015) 12676–12688, https://doi.org/10.1074/jbc.M114.629485, acccessed 2022/01/22
- [29] R.M. Robinson, P.J. Rodriguez, P. Sobrado, Mechanistic studies on the flavin-dependent N6-lysine monooxygenase MbsG reveal an unusual control for catalysis, Arch. Biochem. Biophys. 550–551 (2014) 58–66, https://doi.org/10.1016/j.abb.2014.04.006.
- [30] L.K. Siddens, S.K. Krueger, M.C. Henderson, D.E. Williams, Mammalian flavincontaining monooxygenase (FMO) as a source of hydrogen peroxide, Biochem. Pharmacol. 89 (1) (2014) 141–147, https://doi.org/10.1016/j.bcp.2014.02.006. From NLM.
- [31] J.W. Hill, R.B. Coy, P.E. Lewandowski, Oxidation of cysteine to cystine using hydrogen peroxide, J. Chem. Educ. 67 (2) (1990) 172, https://doi.org/10.1021/ ed067p172.
- [32] J.M. Roscoe, C.S. Sevier, Pathways for sensing and responding to hydrogen peroxide at the endoplasmic reticulum, Cells 9 (10) (2020) 2314.
- [33] N.S. Lyons, A.N. Bogner, J.J. Tanner, P. Sobrado, Kinetic and structural characterization of a flavin-dependent putrescine N-hydroxylase from acinetobacter baumannii, Biochemistry 61 (22) (2022) 2607–2620, https://doi. org/10.1021/acs.biochem.2c00493.
- [34] N.B. Beaty, D.P. Ballou, The reductive half-reaction of liver microsomal FADcontaining monooxygenase, J. Biol. Chem. 256 (9) (1981) 4611–4618, https://doi. org/10.1016/S0021-9258(19)69479-2.
- [35] C. Shirey, S. Badieyan, P. Sobrado, Role of ser-257 in the sliding mechanism of NADP(H) in the reaction catalyzed by the Aspergillus fumigatus flavin-dependent ornithine N5-monooxygenase SidA, J. Biol. Chem. 288 (45) (2013) 32440–32448, https://doi.org/10.1074/ibc.M113.487181.
- [36] A. Alfieri, E. Malito, R. Orru, M.W. Fraaije, A. Mattevi, Revealing the moonlighting role of NADP in the structure of a flavin-containing monooxygenase, Proc. Natl. Acad. Sci. USA 105 (18) (2008) 6572–6577, https://doi.org/10.1073/ pnas.0800859105.
- [37] A. Chang, T. Hartmann, Solubilization and characterization of a senecionine N-oxygenase from Crotalaria scassellatii seedlings, Phytochemistry 49 (7) (1998) 1859–1866, https://doi.org/10.1016/S0031-9422(98)00396-3.
- [38] C.R. Nicoll, G. Bailleul, F. Fiorentini, M.L. Mascotti, M.W. Fraaije, A. Mattevi, Ancestral-sequence reconstruction unveils the structural basis of function in mammalian FMOs, Nat. Struct. Mol. Biol. 27 (1) (2020) 14–24, https://doi.org/ 10.1038/s41594-019-0347-2.
- [39] B.A. Palfey, C.A. McDonald, Control of catalysis in flavin-dependent monooxygenases, Arch. Biochem. Biophys. 493 (1) (2010) 26–36, https://doi.org/ 10.1016/j.abb.2009.11.028.
- [40] T. Spector, V. Massey, Studies on the effector specificity of p-hydroxybenzoate hydroxylase from Pseudomonas fluorescens, J. Biol. Chem. 247 (14) (1972) 4679–4687.